Available online at http://www.nrjp.co.in

Journal of Industrial Relationship, Corporate Governance &Management Explorer, (e ISSN 2456-9461)
Vol. 2, Issue, 02. 91-98p, August, 2018

National Research & Journal Publication

Review Article

Dielectric and thermo Behavior of YCMO Manganites Nanoparticles

Dr. Manoj Mittal
Associate Professor,
Shri Ram College, Muzaffarnagar

INTRODUCTION

Since last one decade, multiferroics, exhibiting two or more ferroic orders simultaneously, have attracted considerable interest due to its fascinating magnetoelectric (ME) coupling. In practice, it is difficult to produce genuine multiferroicity due to the complicated and opposite requirements of electronic structure for ferromagnetism (FM) and ferroelectricity (FE), i.e. FM requires un-paired d-electrons while ferroelectricity does not require it. Accordingly, some reports exist on the multiferroicity in few multiferroic oxides, such as $BiFeO_3$ [1, 2], $BiMnO_3$ [3, 4], $RMnO_3$ [5, 6], charge ordered (CO) manganites [7, 8], etc. Vagadia et al have demonstrated the use of $BiFeO_3$ multiferroic in switching devices [1] while Ravalia et al have studied the fundamental origin of multiferroicity in $BiFeO_3$ [2]. Eerenstein et al have studied the effect of synthesis parameters on the high resistive state of pulsed laser deposited (PLD) $BiMnO_3$ films [3]. Iliev et al have studied the electronic structure of orthorhombic $RMnO_3$ manganites [5]. On one hand, Yoshii et al have studied the structural, transport and magnetic properties of CO manganites and observed the size effect on their physical properties [7], on the other hand, Serrao et al have studied the CO manganites from multiferroicity point of view [8].

Amongst all the oxide multiferroic oxides, $RMnO_3$ (R is the rare earth ion or Yttrium ion) manganites have attracted tremendous interest due to a wide variety of physical properties including high resistance insulating state, antiferromagnetism (AFM) and magnetoresistance (MR) exhibited by them [5, 6, 9]. $YMnO_3$ exhibits A-type AFM having frustrated crystal structure, in which Mn ions' spins are arranged in a triangular network within the Mn-O plane and two neighboring Mn ions share another Mn ion as their nearest neighbor [10]. Many reports exist on the studies on $YMnO_3$ manganite for its magnetoelastic behavior [11], electronic structure [12], FE-AFM coupling [13], structure-FE correlations [14], domain

wall structure [15], magnetodielectric (MD) effect [16], magnetism [17], magnetic structure, using neuron diffraction (ND) [18], spin phonon interactions [19], switching behavior [20], etc.

Substitution of divalent/trivalent/tetravalent magnetic and non-magnetic elements at Mn-site in $YMnO_3$ modifies its transport, electrical, dielectric and magnetic properties [21 – 25]. Gutierrez et al have observed Cu^{2+} substitution induced structural phase transition in $YMn_{1-x}Cu_xO_3$ [21] while at the same time, Moure et al have discussed the phase transition in $YMn_{1-x}M_xO_3$ (M = Cu, Ni & Co) and its dependence on size disorder and tolerance factor [22]. Studies from the view point of multiferroicity, Aikawa et al have reported the effect of Ti^{4+} at Mn-site in $YMnO_3$ and found the structural phase transition and strong MD behavior [24]. In addition, modifications in multiferroicity in $YMnO_3$ have also been studied using the substitution of non-transition metal/non-magnetic Ga^{3+} at Mn-site [25]. Also, few reports are available on the Y-site substitution of Ca^{2+} in $YMnO_3$ studied for their structural, transport, magnetic and dielectric properties [26 – 28].

Nanomaterials, such as nanoparticles, nanorods, nanosized films and nanowires, have unique physical properties, better than their bulk counterparts due to large surface to volume ratio (D^{-1}), which can be critical to the function and integration of nanoscale devices. In this view point, several reports are available on the nanosize effect in $YMnO_3$ based thin films, grown using sol-gel method [29, 30], and nanoparticles, grown using modified citric acid sol-gel method [31] and hydrothermal process [32]. Zhang et al have demonstrated the size effect on the surface structure disorder and hence physical properties of $YMnO_3$ nanoparticles [31] while Zheng et al have reported the spin glassy behavior and exchange bias effect in hexagonal $YMnO_3$ nanoparticles [32].

By keeping in mind, in this communication, the effect of sintering temperature on structure and microstructure and size induced modifications in the dielectric behavior of acetic acid based modified sol-gel grown $Y_{0.95}Ca_{0.05}MnO_3$ nanoparticles have been discussed in the light of grain morphology and oxygen non-stoichiometry.

MATERIALS AND METHODS

Nanoparticles of $Y_{0.95}Ca_{0.05}MnO_3$ (YCMO) manganites were grown using acetic acid based modified sol-gel method, as discussed earlier [33, 34]. Metal acetates of Y, Ca and Mn were dissolved in acetic acid and double distilled water (having 1:1 ratio) in a beaker with continuous stirring to make 0.3M solution which was dehydrated at 90^oC to form a sol, subjected to further slow heating at 150^oC to obtain a gel. The resultant gel was then heated slowly for long time at 150^oC and brown powder was calcined at 500^oC for 6 hr. The black calcined powder was then pressed into the pellet form and sintered them at various temperatures, 700, 800, 900, 1000 and 1100^oC in air for 12 hr. Hereafter, YCMO compounds sintered at 700, 800, 900, 1000 and 1100^oC are referred as YC7, YC8, YC9, YC10 and YC11, respectively. X-ray diffraction (XRD) patterns of YCMO compounds were recorded on Philips diffractometer

(PW 3040/60, X'pert PRO) using CuKα radiation at room temperature (RT). Scanning electron microscopy (SEM) measurements were performed on all the samples using secondary electron imaging mode at room temperature. Frequency and temperature dependent dielectric constant (in the range: 80 – 300K up to 100MHz) was measured using Solatron make impedance analyzer.

RESULTS AND DISCUSSION

Figure 1 (a) shows a typical XRD pattern of YC11 sample revealing the single phasic nature without any detectable impurities. All the XRD peaks are identified by their respective *(hkl)* parameters. Figure 1 (b) shows an enlarged view of most intense *(021)* XRD peaks of all the YCMO samples.

It is clearly seen from the Figure 1 (b) that, with increase in sintering temperature (ST), most intense *(021)* peak shifts towards higher angle indicating the decrease in cell volume with ST. Also, the peak intensity decreases while FWHM increases with ST, which suggests that, crystallinity gets improved with ST. Crystallite size (CS) can be calculated using Scherer's formula: $CS = 0.9\lambda/B\cos\theta$, where λ is the wavelength of X-rays used, B is the FWHM and θ is the angle measured. It is found that, CS decreases from YC7 (7.92 nm) to YC11 (70.43 nm).

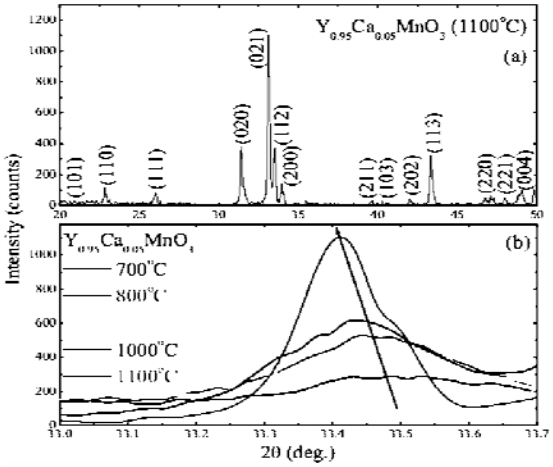

Fig. 1: (a) Typical XRD Pattern of YC11 Sample (b) Enlarged View of Most Intense *(021)* XRD Peaks of all the YCMO Samples.

Figure 2 depicts typical SEM micrographs of nanostructured YC7 and YC11 samples. It can be seen that, with increase in ST, grain size (D) increases with ST, i.e. 125 nm (YC7), 170 nm (YC8), 210 nm (YC9), 265 nm (YC10) and 330 nm (YC11). It is also clear that, with increase in ST, the compactness of the grains increases while in YCMO samples sintered at higher ST possess isolated grain morphology. The grain boundary density (GBD) decreases and the sharpness of the grain boundaries (GB) gets reduced with ST. The corresponding surface to volume ratio (D^{-1}) decreases with ST for the presently studied YCMO samples.

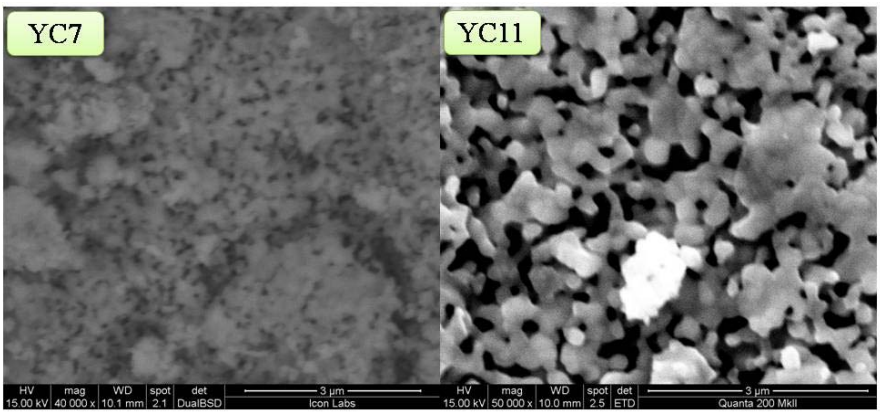

Fig. 2: *Typical SEM Micrographs of Nanostructured YC7 and YC11 Samples.*

Figure 3 shows the variation in dielectric constant (real part: ε´) with frequency for all the nanostructured YCMO samples under study. With increase in frequency, ε´ decreases indicating the relaxor type nature of the samples. For more clarification, inset of Figure 3 shows the log scale of ε´ plots as a function of frequency clearly indicating the increase in ε´ from YC7 to YC11 which can be understood as – Electrical and transport properties of oxide materials depend not only on grain size but also on grain boundary nature [33]. Also it is fact that, oxygen vacancies, located at GB, increases with increase in ST. In the present case of nanostructured YCMO, stoichiometric Mn^{3+}/Mn^{4+} ratio ~ 19 is expected. Due to the oxygen vacancies at grain boundaries, the ratio increases leading to the increase in resistivity of grain boundaries resulting in the large dielectric constant of YCMO samples sintered at higher ST. Dipole polarization obtained in the present case can also be explained by the Maxwell-Wagner model of inhomogeneous dielectric structure [35], which depends on the grain morphology and hence ST.

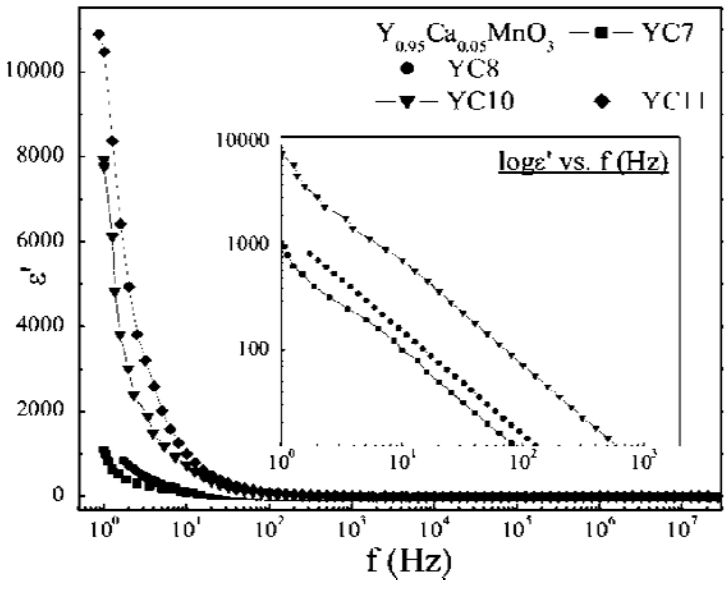

Fig. 3: *Variation in Dielectric Constant (real part: ε´) with Frequency for all the Nanostructured YCMO Samples. Inset: Plots of log scale of ε´ vs. Frequency for all the Nanostructured YCMO Samples.*

Figure 4 shows the variation in dielectric constant (imaginary part: ε´´) with temperature under various frequencies for all the nanostructured YCMO samples studied. It is worth to note that, the large values of ε´´ as compared to ε´ suggests the large dielectric loss across the nanostructured samples, which is found to increase with ST, may be due to the isolated grains and less compact granular growth in higher sintered samples.

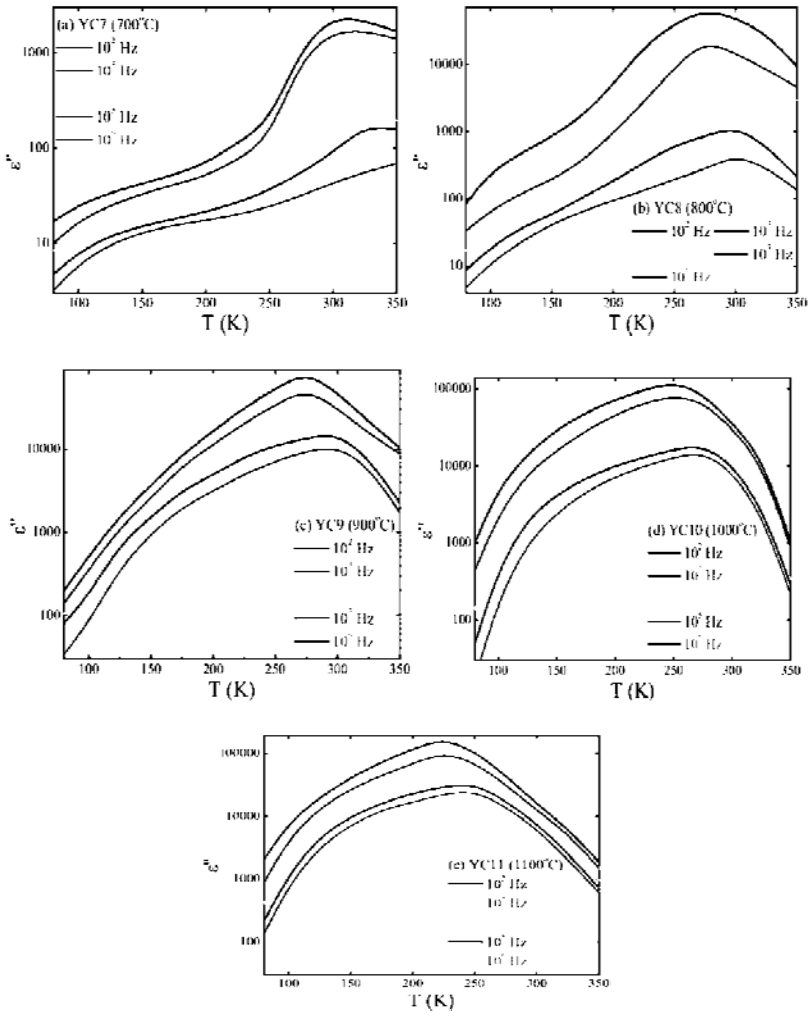

Fig. 4:*Temperature Dependent Dielectric Constant (imaginary part: ε´´) under Various Frequencies for (a) YC7, (b) YC8, (c) YC9, (d) YC10 and (e) YC11 Samples.*

It is clearly seen from Figure 3 (a–e) that, all the samples exhibit dielectric (ε´´) peak which shifts towards higher temperature with increase in frequency while it shifts towards lower temperature [from 311K (YC7) to 225K (YC11)] with increase in ST. From the shifting behavior, one can find the activation energy (E_a) using the formula: $f = f_0 \exp(-E_a/K_BT)$, by plotting the log f vs. 1000/T plots.

Values of E_a can be obtained by fitting the data to straight line, as shown in Figure 5. The values of E_a for all the nanostructured YCMO samples are shown in Figure 5. It can be seen that, E_a increases with ST from 0.97eV (YC7) to 3.79eV (YC11) which can be attributed to the ST induced increase in oxygen deficiency/vacancies leading to the decrease in carrier hoping resulting in the enhancement in E_a with ST.

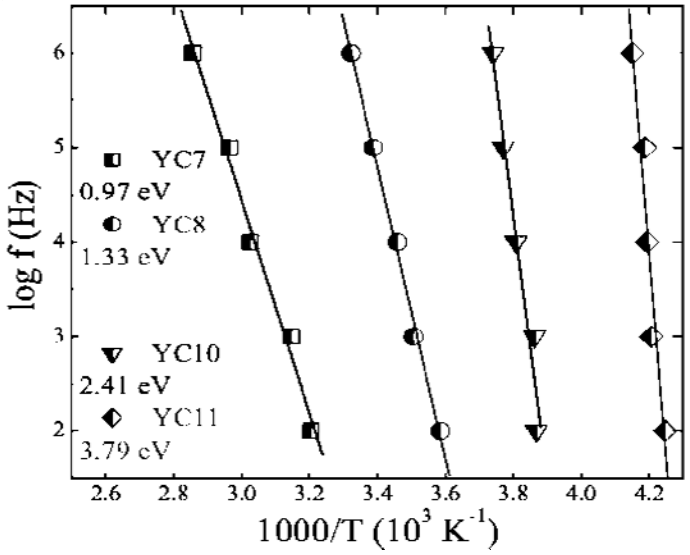

Fig. 5: *Log f versus 1000/T plots for all the Nanostructured YCMO Samples.*

CONCLUSIONS

Nanostructured $Y_{0.95}Ca_{0.05}MnO_3$ samples were grown successfully using low cost acetic acid based modified sol-gel method. The samples were sintered at various sintering temperatures (ST). The crystallinity gets improved while the isolated morphology with higher grain size has been observed on increasing the ST. The grain size increases while grain boundary density decreases with ST which affects the dielectric behavior. In addition, the increase in ST results into the oxygen vacancies in the YCMO nanostructured samples sintered at higher ST, due to which the samples possess larger dielectric constant. Increase in the oxygen vacancies results into the increase in activation energy which has been attributed to the increase in Mn^{3+}/Mn^{4+} ionic ratio and hence decrease in carrier hoping resulting in the enhancement in E_a with ST.

REFERENCES

1. Megha Vagadia, Ashish Ravalia, P.S. Solanki, R.J. Choudhary, D.M. Phase and D.G. Kuberkar, *Appl. Phys. Lett.*. 2013. 103. 033504:1–5p.

2. Ashish Ravalia, Megha Vagadia, Priyanka Trivedi, P.S. Solanki, K. Asokan, S. Ojha, O.P. Thakur, R.J. Choudhary, D.M. Phase and D.G. Kuberkar, *Solid State Commun.*. 2013. 169. 10–13p.

3. W. Eerenstein, F.D. Morrison, J.F. Scott and N.D. Mathur, *Appl. Phys. Lett.*. 2005. 87. 101906:1–3p.

4. H. Chiba, T. Atou and Y. Syono, *J. Solid State Chem.*. 1997. 132. 139–143p.

5. M.N. Iliev, M.V. Abrashev, J. Laverdiere, S. Jandl, M.M. Gospodinov, Y.Q. Wang and Y.Y. Sun, *Phys. Rev. B*. 2006. 73. 064302:1–6p.

6. J.S. Zhou, J.B. Goodenough, J.M. Gallardo-Amores, E. Moran, M.A. Alario-Franco and R. Caudillo, *Phys. Rev. B*. 2006. 74. 014422:1–7p.

7. K. Yoshii, H. Abe and N. Ikeda, *J. Solid State Chem.*. 2005. 178. 3615–3623p.

8. C.R. Serrao, A. Sundaresan and C.N.R. Rao, *J. Phys.: Condens. Matter*. 2007. 19. 496217:1–5p.

9. A. Munoz, J.A. Alonso, M.J. Martinez-Lope, M.T. Casais, J.L. Martinez and M.T. Fernandez-Diaz, *Phys. Rev. B*. 2000. 62. 9498–9510p.

10. V. Laukhin, V. Skumryev, X. Marti, D. Hrabovsky, F. Sanchez, M.V. Garcia-Cuanca, C. Ferrater, M. Varela, U. Luders, J.F. Bobo and J. Fontcuberta, *Phys. Rev. Lett.*. 2006. 97. 227201:1–4p.

11. A.K. Singh, S. Patnaik, S.D. Kaushik and V. Siriguri, *Phys. Rev. B*. 2010. 81. 184406:1–6p.

12. O. Treu Filho, J.C. Pinheiro, R.T. Kondo, R.F.C. Mar, C.O. Paiva-Santos, M.R. Davolos and M. Jafelicci Jr., *J. Molecular Structure*. 2003. 629. 21–26p.

13. Z.J. Huang, Y. Cao, Y.Y. Sun, Y.Y. Xue and C.W. Chu, *Phys. Rev. B*. 1997. 56. 2623–2626p.

14. S.C. Abrahams, *Acta Cryst. B*. 2001. 57. 485–490p.

15. M. Fiebig, A.V. Goltsev, Th. Lottermoser and R.V. Pisarev, *J. Magn. Magn. Mater.* 2004. 272. 353–354p.

16. B. Lorenz, Y.Q. Wang, Y.Y. Sun and C.W. Chu, *Phys. Rev. B*. 2004. 70. 212412:1–4p.

17. A. Munoz, J.A. Alonso, M.T. Casais, M.J. Martinez-Lope, J.L. Martinez and M.T. Fernandez-Diaz, *J. Phys.: Condens. Matter*. 2002. 14. 3285–3294p.

18. P.J. Brown and T. Chatterji, *J. Phys.: Condens. Matter*. 2006. 18. 10085–10096p.

19. P.A. Sharma, J.S. Ahn, N. Hur, S. Park, S.B. Kim, S. Lee, J.-G. Park, S. Guha and S.-W. Cheong, *Phys. Rev. Lett.*. 2004. 93. 177202:1–4p.

20. C. Moure, J.F. Fernandez, M. Villegas and P. Duran, *J. Euro. Ceram. Soc.*. 1999. 19. 131–137p.

21. D. Gutierrez, O. Pena, P. Duran and C. Moure, *J. Eur. Ceram. Soc.*. 2002. 22. 2939–2944p.

22. C. Moure, D. Gutierrez, O. Pena and P. Duran, *J. Solid State Chem.*. 2002. 163. 377–384p.

23. A. Veres, J.G. Noudem, S. Fourrez and G. Bailleul, *Solid State Sci.*. 2006. 8. 137–141p.

24. Y. Aikawa, T. Katsufuji, T. Arima and K. Kato, *Phys. Rev. B*. 2005. 71. 184418:1–5p.

25. H.D. Zhou, J.C. Denyszyn and J.B. Goodenough, *Phys. Rev. B*. 2005. 72. 224401:1–5p.

26. M.N. Iliev, B. Lorenz, A.P. Litvinchuk, Y.Q. Wang, Y.Y. Sun and C.W. Chu, *J. Phys.: Condens. Matter*. 2005. 17. 3333–3342p.

27. J.R. Sahu, C.R. Serrao, A. Ghosh, A. Sundaresan and C.N.R. Rao, *Solid State Commun.*. 2009. 149. 49–51p.

28. Y. Su, Z. Chen, Y. Li, D. Deng, S. Cao and J. Zhang, *J. Supecond. Nov. Magn.*. 2010. 23. 501–506p.

29. K. Tadanaga, H. Kitahata, T. Minami, N. Fujimura and T. Ito, *J. Sol-Gel Sci. Technol.*. 1998. 13. 903–908p.

30. G. Teowee, K.C. McCarthy, F.S. McCarthy and T.J. Bukowski, *J. Sol-Gel Sci. Technol.*. 1998. 13. 899–902p.

31. M.F. Zhang, J.-M. Liu and Z.G. Liu, *Appl. Phys. A*. 2004. 79. 1753–1756p.

32. H.W. Zheng, Y.F. Liu, W.Y. Zhang, S.J. Liu, H.R. Zhang and K.F. Wang, *J. Appl. Phys.*. 2010. 107. 053901:1–4p.

33. P.S. Solanki, R.R. Doshi, C.M. Thaker, Swati Pandya, V. Ganesan and D.G. Kuberkar, *J. Nanosci. Nanotechnol.*. 2009. 9. 5681–5686p.

34. D.G. Kuberkar, R.R. Doshi, P.S. Solanki, Uma Khachar, Megha Vagadia, Ashish Ravalia and V. Ganesan, *Appl. Sur. Sci.*. 2012. 258. 9041–9046p.

35. K.W. Wagner, *Am. J. Phys.* 1973. 40. 317p.